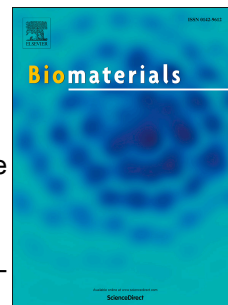


Accepted Manuscript

Synthetic Virus-like Particles Prepared via Protein Corona Formation Enable Effective Vaccination in an Avian Model of Coronavirus Infection

Hui-Wen Chen, Chen-Yu Huang, Shu-Yi Lin, Zih-Syun Fang, Chen-Hsuan Hsu, Jung-Chen Lin, Yuan-I. Chen, Bing-Yu Yao, Che-Ming J. Hu



PII: S0142-9612(16)30404-5

DOI: [10.1016/j.biomaterials.2016.08.018](https://doi.org/10.1016/j.biomaterials.2016.08.018)

Reference: JBMT 17665

To appear in: *Biomaterials*

Received Date: 15 May 2016

Revised Date: 10 August 2016

Accepted Date: 13 August 2016

Please cite this article as: Chen H-W, Huang C-Y, Lin S-Y, Fang Z-S, Hsu C-H, Lin J-C, Chen Y-I, Yao B-Y, Hu C-MJ, Synthetic Virus-like Particles Prepared via Protein Corona Formation Enable Effective Vaccination in an Avian Model of Coronavirus Infection, *Biomaterials* (2016), doi: 10.1016/j.biomaterials.2016.08.018.

This is a PDF file of an unedited manuscript that has been accepted for publication. As a service to our customers we are providing this early version of the manuscript. The manuscript will undergo copyediting, typesetting, and review of the resulting proof before it is published in its final form. Please note that during the production process errors may be discovered which could affect the content, and all legal disclaimers that apply to the journal pertain.

1 Synthetic Virus-like Particles Prepared via Protein Corona
2 Formation Enable Effective Vaccination in an Avian Model of
3 Coronavirus Infection

4 *Hui-Wen Chen^{†§*}, Chen-Yu Huang^{†‡}, Shu-Yi Lin[†], Zih-Syun Fang^{†‡}, Chen-Hsuan Hsu[†], Jung-*
5 *Chen Lin[‡], Yuan-I Chen[‡], Bing-Yu Yao[‡], Che-Ming J. Hu^{§†*}*

6 †Department of Veterinary Medicine, National Taiwan University, Taipei, Taiwan

7 ‡Institute of Biomedical Sciences, Academia Sinica, Taipei, Taiwan

8 §Research Center for Nanotechnology and Infectious Diseases, Taipei, Taiwan

9

10 *Corresponding authors. Email: chu@ibms.sinica.edu.tw; winnichen@ntu.edu.tw

11

12

13 KEYWORDS

14 Protein corona, virus-like particles, gold nanoparticles, coronavirus, infectious bronchitis virus,
15 spike proteins.

16

17

18

19

20

21

22

23 **ABSTRACT**

24 The ongoing battle against current and rising viral infectious threats has prompted increasing
25 effort in the development of vaccine technology. A major thrust in vaccine research focuses on
26 developing formulations with virus-like features towards enhancing antigen presentation and
27 immune processing. Herein, a facile approach to formulate synthetic virus-like particles (sVLPs)
28 is demonstrated by exploiting the phenomenon of protein corona formation induced by the high-
29 energy surfaces of synthetic nanoparticles. Using an avian coronavirus spike protein as a model
30 antigen, sVLPs were prepared by incubating 100 nm gold nanoparticles in a solution containing
31 an optimized concentration of viral proteins. Following removal of free proteins, antigen-laden
32 particles were recovered and showed morphological semblance to natural viral particles under
33 nanoparticle tracking analysis and transmission electron microscopy. As compared to inoculation
34 with free proteins, vaccination with the sVLPs showed enhanced lymphatic antigen delivery,
35 induced stronger antibody titers, increased splenic T-cell response, and reduced infection-
36 associated symptoms in an avian model of coronavirus infection. Comparison to a commercial
37 whole inactivated virus vaccine also showed evidence of superior antiviral protection by the
38 sVLPs. The study demonstrates a simple yet robust method in bridging viral antigens with
39 synthetic nanoparticles for improved vaccine application; it has practical implications in the
40 management of human viral infections as well as in animal agriculture.

41

42

43

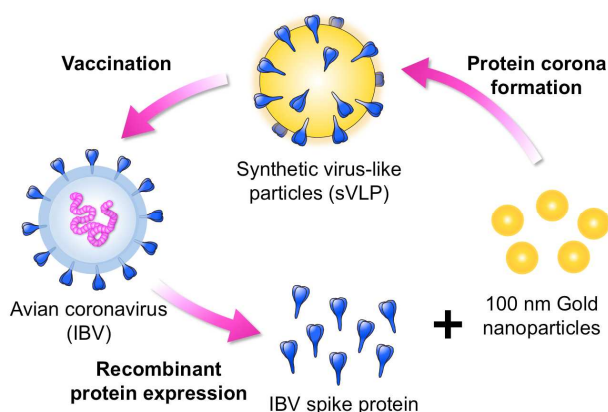
44 1. INTRODUCTION

45 Vaccine is historically the most effective countermeasure against infectious threats, as
46 agents resembling pathogens are administered to mount an immune response against specific
47 targets. Amidst continuing and emerging viral threats, vaccine technology continues to advance
48 with the aim of effectively promoting antiviral immune responses, and a major development
49 effort lies in retaining or integrating virus-like features in vaccine formulations for improved
50 immune processing. Several morphological and antigenic characteristics of viral particles have
51 been demonstrated to promote immune potentiation. For example, particles at the nanoscale have
52 been shown to have better lymphatic transport as compared to smaller subunit antigens [1, 2]. In
53 addition, the display of multiple antigens on a single particle facilitates more effective antigen
54 presentation to immune cells [1]. As compared to traditional vaccine formulations, vaccines
55 preserving virus-like features have shown superior capability in eliciting immune responses [3-
56 5]. These results and observations have also prompted material scientists to apply synthetic
57 nanomaterials towards mimicking viral features for vaccine development [6-9].

58 Given their high radii of curvature, synthetic nanoparticles frequently possess high
59 surface energies that induce adsorption of biomolecules in a phenomenon known as protein
60 corona formation. In protein-rich media, strong nanoparticle/protein association occurs
61 spontaneously as a means to passivate surface energies, and the resulting particles are encased in
62 a protein layer that dictates the particles' interactions with the environment [10, 11]. While
63 protein corona formation is gaining increasing scientific interest owing to its implications in
64 biomedical applications [10, 12, 13], we herein demonstrate harnessing this phenomenon can be
65 beneficial towards mimicking viral features for vaccine applications. We show that synthetic
66 virus-like particles (sVLPs) with close semblance to native virions in physicochemical properties

67 and antigen display can be facilely prepared through spontaneous antigen-particle association in
68 optimized incubation conditions. Using 100 nm gold nanoparticles (AuNP), a biologically inert
69 material commonly used for biomedical research [14-16], and a spike glycoprotein derived from
70 an avian infectious bronchitis virus (IBV), a single-stranded positive-sense RNA virus that
71 belongs to the family *Coronaviridae* [17], we controlled the incubation condition to prepare
72 spike glycoprotein-laden sVLPs (Figure 1). The morphological features and antigen display by
73 the sVLPs were compared to native IBV viral particles using nanoparticle tracking analysis and
74 immunogold staining. In addition, vaccination potency between the sVLPs and free spike
75 glycoproteins was compared in an avian model of coronavirus infection. A commercial whole
76 inactivated virus (WIV) formulation that is the current standard vaccine for IBV management
77 was examined in parallel.

78 Coronaviruses are a major viral family of which the most publicized examples include
79 the pathogens behind severe acute respiratory syndrome coronavirus (SARS-CoV) and Middle
80 East respiratory syndrome coronavirus (MERS-CoV)[18]. In animals, IBV is a prime example of
81 coronavirus that infects the respiratory and urogenital tracts of chickens, posing a serious
82 economic threat as one of the most important pathogens in the poultry industry. The IBV spike
83 glycoprotein, which forms the large, pental-shaped spikes on the surface of the virion, is chosen
84 as the antigen candidate as it is implicated as a determinant of virus pathogenicity. Among
85 coronaviruses, spike glycoproteins possess a variety of biological functions, including triggering
86 cell attachment, inducing cell-cell fusion, and binding to cellular receptors [19, 20]. As spike
87 glycoproteins are the primary targets in ongoing vaccine development efforts for coronavirus
88 vaccinations, the present study has broad implications across both human and animal disease
89 management [21, 22].



90

91 **Figure 1. Schematics illustrating the preparation of an avian coronavirus sVLPs.** sVLPs are
 92 prepared in optimized mixtures containing viral proteins and 100 nm gold nanoparticles via
 93 spontaneous protein corona formation.

94

95 2. MATERIALS AND METHODS

96 2.1 Cells and gold nanoparticles

97 *S. frugiperda* Sf9 (ATCC CRL-1711) insect cells were cultured in Grace's insect cell medium
 98 (Invitrogen, Carlsbad, CA) and supplemented with 10% FBS (Thermo Fisher, Rockford, IL) and
 99 1% P/S/A antibiotics (Biological Industries, Beit-Haemek, Israel) at 27°C. 100 nm gold
 100 nanoparticle (AuNP) solution was purchased from Sigma-Aldrich (St. Louis, MO).

101 2.2 Propagation of IBV

102 Avian coronavirus IBV strain 2575/98 was propagated in 10-day-old specific-pathogen-free
 103 (SPF) chicken embryos via the allantoic route as previously described [23]. The virus titers of
 104 IBVs were determined with the method of Reed and Muench [24] in SPF chicken embryos and
 105 expressed as 50% embryo infectious dose (EID₅₀)[25]. The virus-containing allantoic fluid was

106 concentrated and purified using sucrose gradient solution as previously described to derive the
107 native virions [23].

108 **2.3 Preparation of recombinant IBV spike proteins**

109 Full spike (S) protein of avian coronavirus IBV was cloned and expressed using the Bac-to-Bac
110 baculovirus expression system (Invitrogen). Briefly, a recombinant plasmid was constructed by
111 inserting full spike protein gene of IBV strain 2575/98 (accession no. DQ646405)[26] into the
112 pFastBac-1 vector using the following primer set: IBV-S-BamHI-f: 5'- TTGGG ATCCG
113 ATGTT GGTGA AGTCA C-3'; IBV-S-SalI-f: 5'-CTTGT CGACA TTAAA CAGAC TTTT
114 AGGT-3'. The recombinant pFastBac-1 shuttle vector was then transposed to the bacmid in *E.*
115 *coli* strain DH10Bac, and recombinant bacmid was purified using the HiPure Plasmid Midiprep
116 kit (Invitrogen). Sf9 cells were used for transfection with the recombinant bacmid, and
117 recombinant baculoviruses were then harvested in the supernatant and designated rBac-2575S.
118 Recombinant spike proteins (r2575S) were harvested from Sf9 cells infected with rBac-2575S
119 (multiplicity of infection =1). Sf9 cells were washed and lysed with the I-PER insect cell protein
120 extraction reagent (Thermo Fisher). Recombinant proteins were purified using the Glycoprotein
121 Isolation Kit, ConA (Thermo Fisher) according to the manufacturer's instructions. After
122 purification, r2575S protein was stored in 10% sucrose at -20°C.

123 **2.4 Preparation of synthetic virus-like particles**

124 Citrate-buffered 100 nm gold nanoparticles were washed repeatedly in water to remove the
125 citrate stabilizer, and the resulting pellet was resuspended in 10% sucrose. Protein solutions
126 ranging in concentrations between 100 µg/mL to 3 mg/mL of purified spike proteins were then
127 mixed with 1×10^{11} /mL of gold nanoparticles (determined by nanoparticle tracking analysis) in
128 10% sucrose. The mixtures were bath sonicated for 1 min followed by incubation in an ice bath

129 for 30 min. The nanoparticles were then removed from unbound spike proteins via centrifugation
130 at 1500×g for 3 min. Following 3 centrifugal washes with 10% sucrose, pelleted nanoparticles
131 were mixed with 1× PBS and sonicated in a bath sonicator for 30 sec. Dispersible, stabilized
132 sVLPs were retrieved and their protein content was quantified using a BCA protein assay
133 (Thermo Fisher) with 25 μL of 1×10^{11} particles/mL following the manufacturer's protocol.
134 Visualization of unstable nanoparticles and colloiddally stable sVLPs was performed using a 200
135 kV high resolution transmission electron microscope (FEI Tecnai TF20). Particle stability was
136 assessed by monitoring the size of sVLPs for 7 days. Particle size, polydispersity index (PDI),
137 and concentrations were measured by nanoparticle tracking analysis using Nanosight NS-500
138 (Malvern, UK) at a concentration of 1×10^8 particles/mL based on the manufacturer's
139 instructions. Particle size and zeta potential were also measured by dynamic light scattering
140 using Zetasizer Nano ZS at a concentration of 1×10^{10} particles/mL (Malvern, UK) based on the
141 manufacturer's instructions.

142 **2.5 Examination of antigen display and retention**

143 Antigen display was examined using freshly prepared sVLPs. Antigen retention was examined
144 by mixing sVLPs in protein-poor (PBS) or in protein-rich (10% BSA) conditions for varying
145 periods of time. At 0, 3, 10, and 24 hr marks, sVLPs were pelleted from their respective
146 solutions. The particles were then processed using a previously published protocol with SDS-
147 PAGE loading buffer for protein removal and quantification [27]. IBV spike proteins eluted from
148 the sVLP were analyzed in 6% discontinuous SDS-PAGE under non-reducing condition. Protein
149 gel was then transferred onto a 0.45 μm nitrocellulose membrane (Bio-Rad). After transfer, the
150 membrane was soaked in blocking buffer (5% skim milk in PBS) at room temperature for 1 hr
151 and probed with anti-S monoclonal antibody (mAb) for another 1 hr. After three washes, the

152 membrane was incubated with peroxidase-conjugated goat anti-mouse IgG (H+L) (Jackson
153 ImmunoResearch Laboratories, West Grove, PA) in blocking buffer at room temperature for 1
154 hr. After three washes, the protein blots were detected with either TMB Membrane Peroxidase
155 Substrate (KPL) or enhanced chemiluminescence (ECL) substrate (Pierce). Band intensities were
156 analyzed via imaging analysis using ImageJ. Presence of IBV spike proteins on the sVLPs was
157 further verified by immunogold staining, and purified IBV 2575/98 virions were used as a
158 control. Briefly, 3 μ l of sVLP or virion samples were deposited onto a glow-discharged carbon-
159 coated grid for 2 min. The virion sample was fixed with 4% paraformaldehyde for 5 min. After 3
160 washes with PBS, the samples were blocked with 1% BSA for 15 min. The samples were then
161 incubated with anti-S mAb for 1 hr. After PBS washes, the samples were incubated with 6 nm
162 gold-conjugated goat anti-mouse IgG (Jackson ImmunoResearch Laboratories) for another 1 hr.
163 After PBS washes, native virions were further stained with 1% uranyl acetate for 15 sec. All
164 experiments were performed at room temperature. Particles were visualized under a 200 kV high
165 resolution transmission electron microscope (FEI Tecnai TF20).

166 **2.6 Antigen delivery quantification**

167 The care and use of animals were approved by the Institute Animal Care and Use Committee,
168 National Taiwan University (approval no. NTU-102-EL-89). All animal experiments were
169 carried out in accordance with the approved guidelines. 8-week old BALB/c mice were injected
170 with 50 μ L of PBS, free protein formulation, or sVLPs containing 2 μ g of viral antigens via the
171 intra-footpad route. After 24 hr, the mice were sacrificed and the popliteal lymph nodes were
172 harvested (n = 6). Cryosections (6 μ m) were made and fixed for 10 min in acetone, followed by 8
173 min in 1% paraformaldehyde. Sections were blocked by 5% normal goat serum (Invitrogen) in
174 PBS for 10 min and stained with anti-S mAb for 4 hr at room temperature. After washes,

175 sections were further incubated with FITC-conjugated anti-mouse IgG (Jackson
176 ImmunoResearch Laboratories) for 1 hr at room temperature. Nuclei were counterstained with
177 DAPI (Invitrogen). Fluorescence signal was observed under a fluorescence microscope (Leica
178 DMI8), and quantified via imaging analysis using ImageJ.

179 **2.7 Animal immunization**

180 8-week old BALB/c mice were injected intramuscularly in the thigh with 100 μ L of formulations
181 containing PBS, free protein, or sVLPs (10 μ g of viral antigens) mixed with the complete
182 Freund's adjuvant. Mice blood was collected on day 14 and 21 for antibody titer quantification
183 (n = 4-5 per group). Three-week-old SPF chickens were obtained from JD-SPF Biotech (Miaoli,
184 Taiwan). Chickens were randomly divided into four different experimental groups (n = 4-6 per
185 group) receiving PBS, free protein (r2575S), whole inactivated virus (WIV) vaccine (Merial
186 Laboratories, Lyon, France), or sVLPs. Briefly, free protein or sVLPs (10 μ g of viral antigen in
187 100 μ L) were emulsified with the complete Freund's adjuvant and administered via an
188 intramuscular route. The commercially available WIV vaccine (oily-adjuvanted) was
189 administered to chickens according to the manufacturer's recommendation (0.3 ml per chick).
190 Chicken sera and tears were collected on day 0 (before immunization), 14, and 21 post-
191 immunization. All chickens were intranasally challenged with IBV 2575/98 live virus (10^6 EID₅₀)
192 on day 21, and were observed for disease signs for 7 days. Chickens were sacrificed on day 28.

193 **2.8 Antibody quantification**

194 For serum IgA and IgG virus-specific ELISA, 100 ng of purified IBV 2575/98 virions was
195 diluted with coating buffer (15 mM Na₂CO₃ and 35 mM NaHCO₃, pH 9.6) and coated onto flat-
196 bottomed microtiter plates (Nunc) at room temperature overnight. The wells were washed with
197 PBST (0.1% Tween 80 in PBS) three times and blocked with blocking reagent (5% skim milk in

198 PBST) at 37 °C for 1 hr. After washes, 100 µl of chicken serum was added and incubated at room
199 temperature for 1 hr. Following three washes, 100 µl of peroxidase-conjugated goat anti-chicken
200 IgY (H+L) or IgA (Jackson ImmunoResearch) in blocking buffer was added into each well and
201 incubated at room temperature for 1 hr. After three washes, 100 µl of SureBlue Reserve TMB
202 Microwell Peroxidase Substrate (KPL) was added to each well and incubated in the dark at room
203 temperature for 10 min. The reaction was stopped by adding 100 µl of TMB stop solution (KPL).
204 The OD was measured at 450 nm using an automated plate reader (Thermo Fisher). For total tear
205 IgA quantification, ELISA was performed with Chicken IgA ELISA Kit (ab157691, Abcam)
206 according to the manufacturer's protocol.

207 **2.9 Antigen-specific cytokine expression analysis**

208 On day 28 post immunization, chicken spleens were minced and passed through a 70-µm cell
209 strainer (Corning) to obtain single-cell suspensions. Red blood cells (RBCs) were lysed using an
210 RBC lysis buffer (eBiosciences), and cells were resuspended in RPMI 1640 medium (Gibco,
211 Grand Island, NY) containing 10% FBS. Viable cells were determined by trypan blue staining.
212 10⁶ splenocytes were plated in 96-well U-bottom plates (Corning), and were stimulated with 1 µg
213 of purified IBV 2575/98 virions in the presence of brefeldin A (GolgiPlug, BD Biosciences) for
214 6 hr at 37°C. For the quantification of cytokine expression, the stimulated splenocytes were
215 lysed, and total RNA was isolated by TRIzol (Invitrogen) according to the manufacturer's
216 manual. Real-time RT-PCR was performed using iScript (Bio-Rad) and iQ SYBR Green
217 Supermix Kit (Bio-Rad) with previously described primers for chicken IFN-γ and GAPDH [28].
218 Melting curve analysis following real-time PCR was conducted to verify the specificity for each
219 primer set. All obtained Ct values were normalized to GAPDH. The relative expression of
220 chicken IFN-γ (fold change of naive control) was determined by a 2^{-ΔΔCt} method [29].

221 **2.10 Clinicopathological assessment**

222 Disease signs of chickens were recorded on a daily basis after virus challenge. The clinical score
223 index of IBV infection was interpreted according to a previously described method [30]. The
224 clinical signs were evaluated as: 0 = no clinical signs; 1 = lacrimation, slight shaking, watering
225 feces or tracheal rales; 2 = lacrimation, presence of nasal exudate, depression, water feces,
226 apparent sneezing or cough; 3 = high degree of lacrimation, nasal exudate, and severe watery
227 feces; 4 = death. After necropsy, gross lesions at the tracheas and kidneys were recorded.
228 Chicken kidneys were further harvested and homogenized in tryptose phosphate broth (BD
229 Biosciences). Viral load in kidneys was assessed by quantitative RT-PCR described below.

230 **2.11 Viral RNA quantification**

231 RNA in chicken kidneys was extracted using TRIzol (Invitrogen) according to the
232 manufacturer's manual. For viral load assessment, Quantitative RT-PCR was performed with
233 iScript (Bio-Rad) and iQ SYBR Green Supermix Kit (Bio-Rad) using previously described
234 primer sets that target the S protein gene of IBV (rC2U and rC3L) [31] and chicken 28S rRNA
235 [32]. Quantitative RT-PCR experiments were performed in duplicates. Data was expressed as
236 arbitrary units.

237 **2.12 Statistical analysis**

238 Data was analyzed by ANOVA followed by Dunnett's multiple comparison tests using
239 GraphPad Prism (GraphPad Software, San Diego, CA). *p* values smaller than 0.05 were
240 considered significant.

241

242 **3. RESULTS AND DISCUSSION**

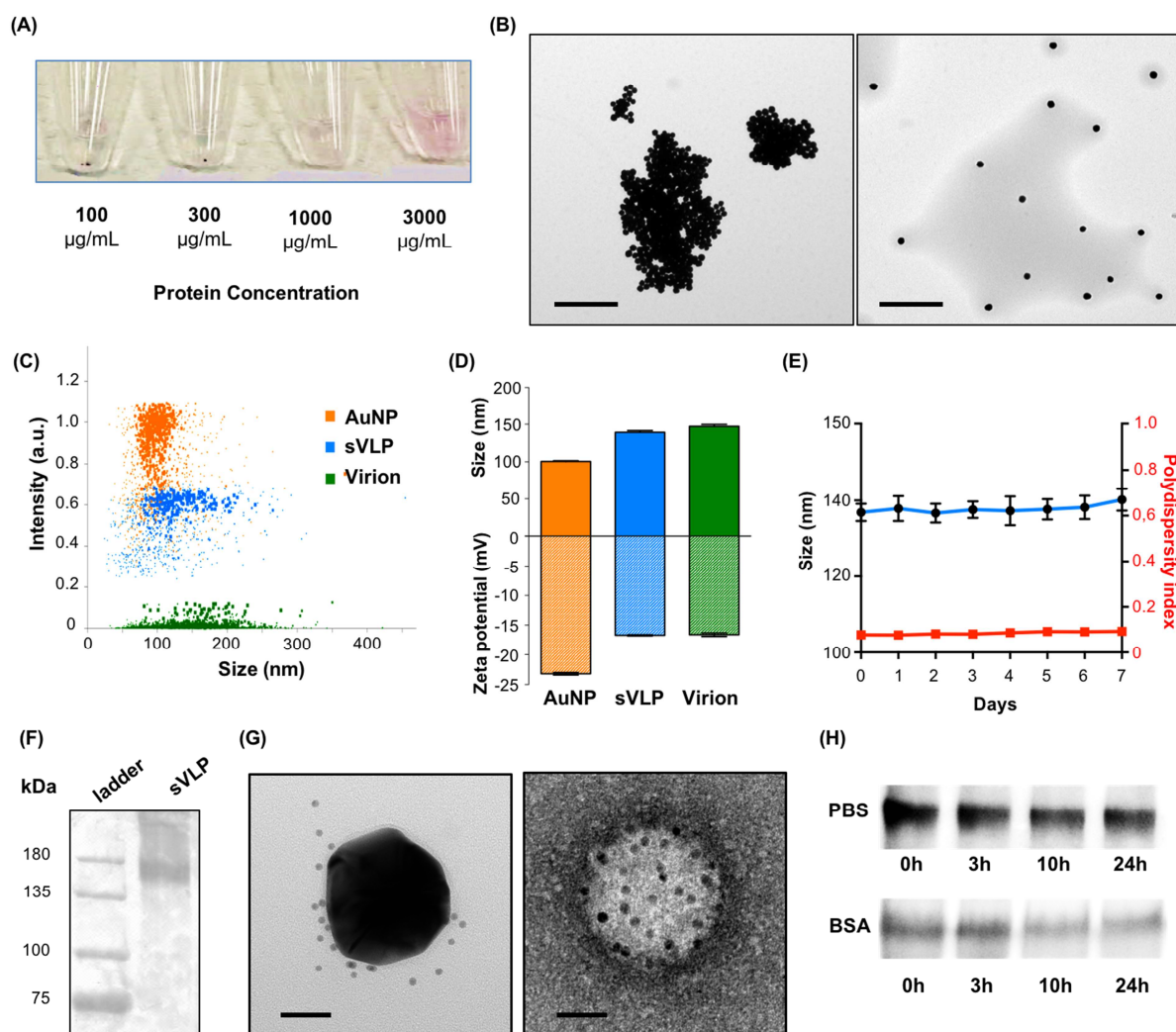
243 Following AuNP incubation in solutions of different protein concentrations, the resulting
244 nanoparticles were pelleted from free proteins and re-dispersed through sonication in PBS.
245 Consistent with previous studies on nanoparticle/protein interactions [33], it was observed that
246 higher protein concentrations yielded particles with increased colloidal stability as evidenced by
247 the disappearance of a discernable pellet and a purple solution characteristic of AuNP
248 suspensions (Figure 2A). sVLPs prepared from the 3 mg/mL protein suspension were readily
249 dispersible and manifest as distinct, non-clustered nanoparticles under transmission electron
250 microscopy (Figure 2B), indicating passivation of the high particle surface energy upon
251 sufficient protein coating. In contrast, particle preparations with lower protein content (1000
252 $\mu\text{g/mL}$) yielded clustered AuNPs. To further characterize sVLPs, we assessed AuNPs, sVLPs,
253 and native IBV virions (Figure 2B) using nanoparticle tracking analysis, which examines particle
254 samples on a particle-by-particle basis via tracking of scattered laser light from individual
255 particles [34]. Between AuNPs and sVLPs, we observed an overall reduction in the light
256 scattering intensity. Given that AuNPs are known to scatter light at an extraordinary efficiency,
257 the intensity reduction in sVLPs can be attributed to successful protein coating, which restricts
258 light passage to the AuNP surfaces. Likewise, native virions have the lowest light scattering
259 under the analysis as they are comprised entirely of organic materials. The result demonstrates
260 the feasibility of studying the evolution of nanoparticle protein corona formation using
261 nanoparticle tracking analysis, which reveals changes in light scattering and size simultaneously.

262 Upon examining the size distributions of the different particles, sVLPs showed a broader
263 distribution as compared to the sharply distributed 100 nm AuNPs. Protein corona formation
264 increased the nanoparticle size from 100.6 nm (PDI = 0.012) to 139.2 nm (PDI = 0.073) and
265 increased the zeta potential from -23.2 mV to -16.7 mV (Figure 2C,D). In comparison to native

266 IBV virions, which have an average diameter of 147.3 nm (PDI = 0.081) and a zeta potential of -
267 16.6 mV, the sVLPs are similar in overall physicochemical properties. Examination of particle
268 stability showed that the sVLPs remained stable in PBS over a 7-day period with its size ranging
269 from 136.7 nm (PDI = 0.071) to 140.2 nm (PDI = 0.091) (Figure 2E). Analysis of antigen
270 display with freshly prepared sVLPs showed that 1×10^{11} AuNPs retained 23.5 ± 2.2 μg of spike
271 proteins, corresponding to approximately 900 IBV spike proteins per particle. Western blotting
272 using analysis revealed a sharp protein band of approximately 160 kDa (Figure 2F), which is
273 characteristic of the viral antigen [17]. Transmission electron microscopy and immunogold
274 staining further highlight the similarity between sVLPs and native IBV virions. It was observed
275 that immunogold clustered around the sVLPs, mirroring the staining pattern on the native virions
276 (Figure 2G). These observations demonstrate the close semblance between the sVLPs and native
277 virions regarding their physicochemical properties and antigen display.

278 Examination of antigen retention in protein-poor (1X PBS) and protein-rich (10% BSA in
279 1X PBS) conditions also shed light on the characteristics of the protein corona around the sVLPs.
280 In PBS, particle-bound antigen level remained steady over a span of 24 hours, yielding similar
281 IBV spike protein band intensities across the different incubation samples (Figure 2H). A rapid
282 drop-off in particle-bound spike protein was observed upon incubation in 10% BSA. Immediate
283 retrieval of sVLPs from the BSA solution resulted in ~65% reduction in spike protein level, and
284 at the 24 hr mark, ~25% of the initial antigen remained on the sVLPs. This observation suggests
285 the formation of two distinctive corona layers distinguishable by their interaction dynamics with
286 surrounding biomolecules, reflecting the presence of both a reversible “soft corona” and an
287 irreversible “hard corona” that have been frequently observed in prior nanoparticle studies [35-
288 37]. The results indicate that approximately 200 to 250 IBV spike proteins are stably bound to

289 each sVLPs. These proteins are expected to remain in the particulate form in complex biological
 290 environments upon *in vivo* administration.



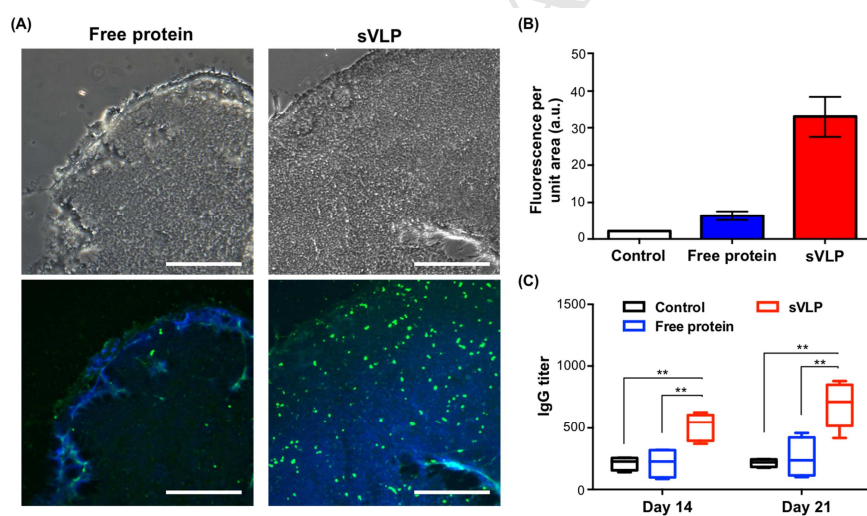
291
 292 **Figure 2. Preparation and characterizations of sVLPs.** (A) Visualization of nanoparticle
 293 solutions following incubation with and isolation from different concentrations of IBV spike
 294 proteins. (B) TEM visualization of nanoparticles prepared with a low protein concentration
 295 (1000 µg/mL; left) and sVLPs prepared with a high protein concentration (3000 µg/mL; right).
 296 Scale bars = 1 µm. (C) Particle-by-particle examination of AuNPs, sVLPs, and native IBV
 297 virions under nanoparticle tracking analysis. (D) Size and zeta potential of AuNPs, sVLPs, and

298 native IBV virions as analyzed by nanoparticle tracking analysis. Bars represent means \pm s.d. (n
299 = 3). (E) sVLP stability in PBS observed over 7 days. Bars represent means \pm s.d. (n = 3). (D)
300 Western blotting analysis confirms the presence of IBV spike proteins on sVLPs. (E)
301 Transmission electron microscopy of sVLPs (left) and native IBV virions (right) following
302 immunogold staining against IBV spike proteins. Scale bars = 50 nm. (H) Western blotting
303 analysis of IBV spike protein retention on sVLPs following different incubation periods in PBS
304 or in 10% BSA.

305

306 To examine antigen delivery and lymphatic transport by the sVLPs as compared to free
307 spike proteins, sVLP formulation was administered to mice through a footpad injection. Popliteal
308 lymph nodes, which are the draining lymph nodes by the footpads, were subsequently collected
309 and sectioned for immunofluorescence assay. IBV spike protein-specific immunofluorescence
310 staining showed a significantly enhanced antigen delivery by the sVLPs as compared to the free
311 protein formulation, resulting in an increased number of fluorescent punctates (green) in the
312 lymph node sections (Figure 3A). Imaging analysis on multiple lymph node sections showed that
313 the sVLP formulation increased lymphatic delivery by approximately 6 fold (Figure 3B). The
314 observation of increased delivery attests to the strong protein/particle binding in the “hard
315 corona” layer as the particle carrier is capable of facilitating antigen transport *in vivo*. The
316 enhanced lymph node localization of the sVLPs is consistent with prior observations on
317 nanoparticles and virus-like particles [2]. Owing to their nanoscale morphology and
318 physicochemical properties, these nanoparticles are known to facilitate free lymphatic drainage
319 via convective transport [38, 39] as well as cell-mediated lymphatic delivery via increased
320 cellular uptake [2].

321 Immunogenicity of the sVLPs was also examined following intramuscular inoculation in
 322 mice. Anti-IBV IgG serum titers were compared between mice vaccinated with sVLPs and with
 323 free IBV spike proteins (Figure 3C), and it was observed that the sVLPs elicited significantly
 324 higher IgG levels, demonstrating improved vaccination potency over the free protein
 325 formulation. The improved immunogenicity can be explained in part by the enhanced antigen
 326 delivery to the lymph node, where a high number of antigen presenting cells reside. In addition,
 327 the particulate nature of the sVLPs likely also favors other immune activation mechanisms, such
 328 as improved cellular uptake, enhanced complement activation [38] and presentation by follicular
 329 dendritic cells [40]. These nanoparticle-specific immunological features make the sVLPs a
 330 promising vaccine candidate for disease management.



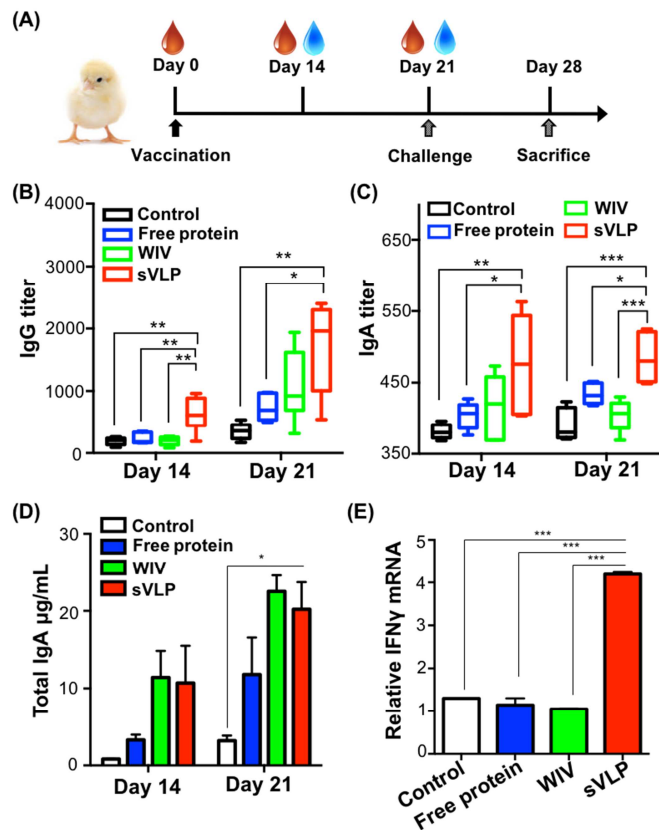
331
 332 **Figure 3. Antigen delivery and immunogenicity of sVLPs.** (A) Sections of popliteal lymph
 333 nodes were examined under bright field (top panel) and using immunofluorescence assay
 334 (bottom panel). Lymph node sections were stained with DAPI (blue) and FITC-conjugated anti-
 335 IBV spike protein antibodies (green) to examine antigen content in the lymph node 24 hr
 336 following footpad injections with free proteins or sVLPs. Scale bars = 100 μ m. (B)

337 Quantification of antigen-specific fluorescence signals in the lymph node. Bars represent means
338 \pm s.d. (n = 6). (C) Quantification of anti-IBV spike protein IgG titers 14 and 21 days following
339 vaccination. Lines and boxes represent upper extreme, 25th, 50th, 75th percentile, and lower
340 extreme (n = 4-5). *P \leq 0.05, **P \leq 0.01, ***P \leq 0.001.

341

342 To evaluate the sVLPs' effectiveness against viral infections, we vaccinated SPF
343 chickens with free IBV spike proteins or sVLPs (10 μ g of total viral antigens) via the
344 intramuscular route. As an additional reference, a commercial WIV vaccine for IBV was
345 administered based on the manufacturer's suggested dosage. Following vaccination, blood and
346 tear were collected for analysis and a live IBV challenge was performed (Figure 4A). ELISA
347 analysis showed that the sVLPs were superior in generating both IgG and IgA titers as compared
348 to the free protein formulation and the WIV vaccine (Figure 4B,C). The total IgA in the tears of
349 the vaccinated chickens were also quantified. Despite that intramuscular vaccination is generally
350 known to be non-ideal for promoting mucosal immunity [41], elevation of tear IgA level was
351 observed for all three vaccine formulations (Figure 4D). It is expected that mucosal vaccination
352 in future studies may further increase tear IgA levels and better highlight the differences among
353 the formulations in eliciting mucosal immunity. Besides humoral immunity, cellular immunity, a
354 major component of effective antiviral immune responses [42], was analyzed using splenocytes
355 extracted on day 28. The sVLP sample showed a significant increase in the IFN- γ mRNA level
356 as compared to the control, free protein, and the WIV vaccine samples (Figure 4E),
357 demonstrating superior promotion of antigen-specific cellular immunity.

358

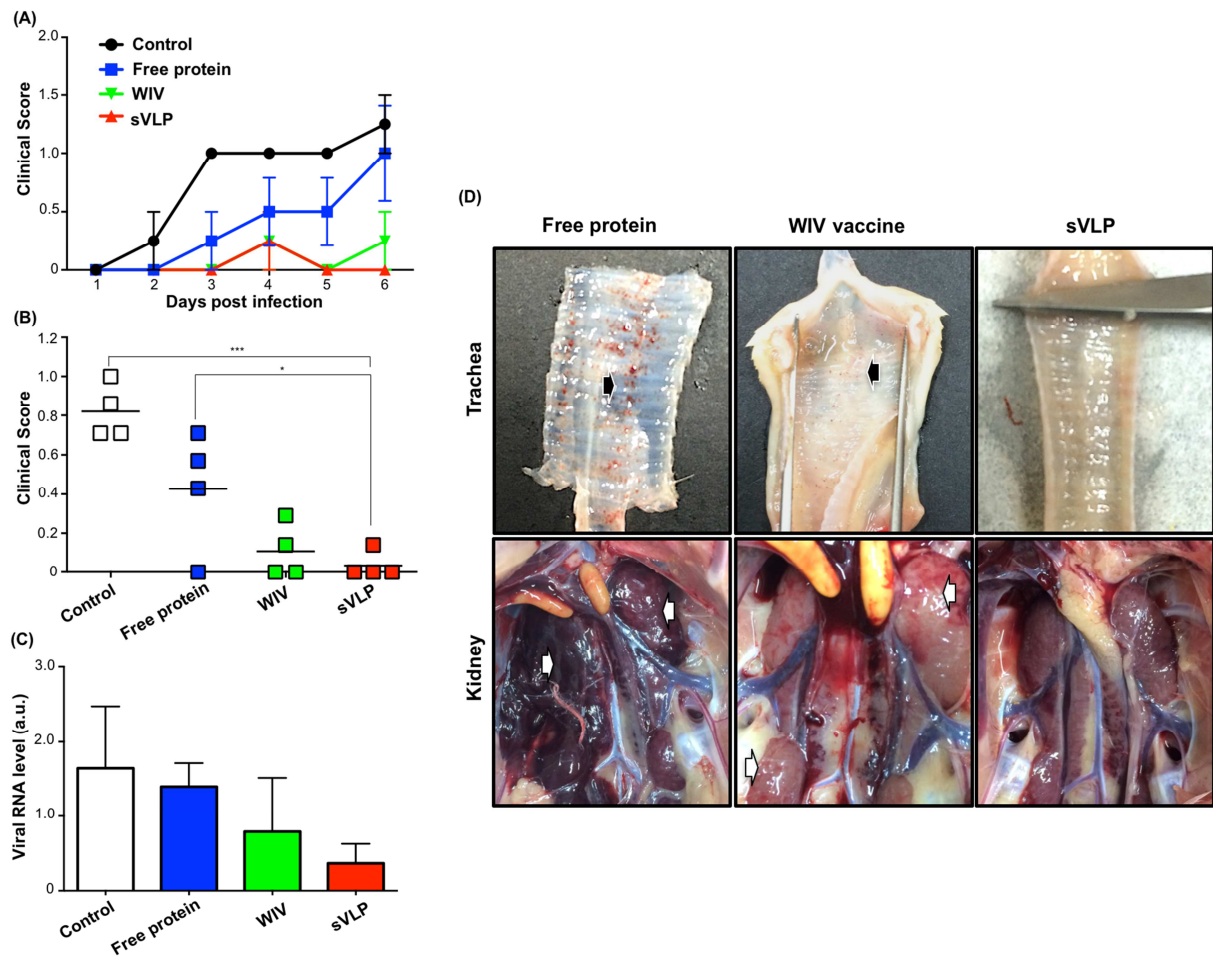


359

360 **Figure 4. Immunopotential following vaccinations with sVLPs.** (A) Vaccination, tissue
 361 sample collection, and virus challenge schedule in an avian model of coronavirus infection. (B)
 362 Virus-specific serum IgG titers observed in animals vaccinated with free proteins, a commercial
 363 whole inactivated virus (WIV) vaccine, and sVLPs. Lines and boxes represent upper extreme,
 364 25th, 50th, 75th percentile, and lower extreme (n = 6). (C) Virus-specific serum IgA titers in
 365 animals vaccinated with the different formulations. Lines and boxes represent upper extreme,
 366 25th, 50th, 75th percentile, and lower extreme (n = 6). (D) Virus-specific tear IgA titers in animals
 367 vaccinated with the different formulations. Bars represent means \pm s.e.m (n = 6). (E) Relative
 368 IFN- γ mRNA levels observed from the splenocytes of the different vaccinated groups following
 369 a viral antigen challenge. Bars represent means \pm s.e.m (n = 4). *P \leq 0.05, **P \leq 0.01, ***P \leq
 370 0.001.

371

372 We further examined the effect of the different vaccinations in protecting against a viral
373 challenge. Clinical scores evaluated based on stamina, posture, and voice show that the sVLP
374 group had the lowest overall symptoms, on par with animals vaccinated with the WIV
375 formulation (Figure 5A,B). In comparison, vaccination with the free protein formulation was less
376 effective and highly variable in moderating the disease symptoms. On day 28, necropsies were
377 performed to examine the tracheas and kidneys, which are characteristic sites for infections by
378 IBV [43]. As indicated in the gross lesion photos, the best antiviral protection was observed in
379 the sVLP-immunized group, whereas organs from the free protein group and the WIV vaccine
380 group showed observable mucus secretion and petechiae in tracheas (Figure 5D, upper panel,
381 arrowed) and swollen lesions and hemorrhages in kidneys (Figure 5D, lower panel, arrowed).
382 The prophylactic effect of the sVLP vaccination was further demonstrated by examining the viral
383 load in kidneys. Analysis by quantitative RT-PCR showed that immunization with sVLPs more
384 consistently reduced the viral content, resulting in the lowest relative viral mRNA expression
385 across the animal samples (Figure 5C). The results further corroborate the enhanced protective
386 effective by the sVLP vaccination, which enhanced both humoral and cellular immunity for
387 increased protection against the viral challenge.



388

389 **Figure 5. Protection against a viral challenge following sVLP vaccination.** (A) Daily clinical
 390 scores of the different vaccinated groups as evaluated by the subjects' stamina, posture, and
 391 voice following IBV viral challenge. (B) Averaged clinical scores over a 6-day observation
 392 period. * $P \leq 0.05$, ** $P \leq 0.01$, *** $P \leq 0.001$. (C) Viral RNA levels in the kidneys of the different
 393 vaccinated samples as measured by quantitative RT-PCR. Bars represent means \pm s.e.m (n = 4).
 394 (D) Necropsies of vaccinated chicken samples following viral challenge by IBV. Examinations
 395 of the trachea (top panel) and kidneys (bottom panel) show different damages reflective of the
 396 viral infection. Petechiae in tracheas and swollen lesions/hemorrhages in kidneys are indicated
 397 by arrows.

398

399 Coronavirus spike proteins are the primary antigenic signatures on coronaviruses as they
400 contribute to the characteristic crown-like morphology underlining this virus family. As these
401 proteins comprise the outermost layer of coronaviruses, the spike proteins have a pivotal role in
402 viral pathogenesis and are recognized as the primary target for vaccine preparations [44].
403 Present vaccination strategies for coronaviruses include recombinant viruses and virus-like
404 particles, and there is a continuing effort in developing new strategies for improving vaccine
405 potency and safety [22]. To the best of our knowledge, incorporating coronavirus spike protein
406 with synthetic nanoparticles has not been previously explored. By exploiting the high surface
407 energies of synthetic nanoparticles, spontaneous assembly of sVLPs covered with IBV spike
408 proteins were demonstrated. The strong particle/antigen association resulted in virus-sized
409 particulates displaying IBV spike proteins, and the sVLPs elicited strong immune protection
410 against a live IBV challenge. The enhanced immunopotentiality by the particle carrier is
411 consistent with previous studies and echoes the curious observation that gold nanoparticles not
412 only promote humoral but also cellular immune responses upon association with antigens [14,
413 15]. As the increased cellular immune response suggests that the nanoparticles may play a role
414 beyond a passive antigen carrier, future studies examining the impact of nanomaterials and
415 nanoparticle surface energies on immunological interactions are warranted.

416 It should be noted that the phenomenon of protein corona formation is an evolving field
417 of study in which scientists continue to examine nanomaterials in biological medium with
418 increasing complexity [45-47]. Subtle changes on the environment and on nanoparticle
419 properties can have dramatic and unpredictable impact on the overall corona identity with
420 significant biological implications. To demonstrate a practical utility for the protein corona

421 phenomenon, the present study adopts a reductionist approach in examining protein-particle
422 interactions. AuNPs are incubated in a highly controlled condition with proteins of a singular
423 species to form sVLPs with virus-mimetic features, and the dynamics of such association are
424 expected to vary with different biomolecules and nanomaterials [48]. In general, inorganic
425 nanoparticles promote stronger protein adsorption as compared to organic nanoparticles as
426 inorganic nanoparticles tend to have higher surface energies. Decreasing particle size also tends
427 to increase biomolecule interactions as it increases radii of curvature of nanoparticle surfaces.
428 Other forces, such as electrostatic interactions, van der Waals forces and covalent interactions all
429 play intertwining roles in governing the nano-bio interface, and factors including nanoparticle
430 functionalizations, buffer conditions, and biomolecule species have significant impact on the
431 corona formation [48]. Nonetheless, in a controlled and optimized condition, the phenomenon
432 may be exploited to facilitate the preparation of formulations with defined characteristics and favorable
433 biological performance. The present work takes advantage of this spontaneous interaction
434 between nanomaterials and biomolecules towards improving vaccine development. This strategy
435 may find practical applications in disease management against coronaviruses as well as other
436 infectious threats.

437

438 **4. CONCLUSIONS**

439 In summary, we demonstrate by incubating viral antigens with synthetic nanoparticles in
440 optimized conditions, spontaneous formation of protein corona induces the assembly of virus-
441 like nanostructures with viral antigens encasing the particulate core. Results from the present
442 study validate the successful preparation of sVLPs via nanoparticles' innate tendency to induce

443 protein coating. In comparison to typical virus-like particle preparations, the present strategy
444 offers practical advantages owing to its simple and facile process. Amidst the growing health
445 threats of coronavirus infections as well as the ongoing economic impact of IBV infections,
446 virus-like particles are garnering increasing scientific interest as vaccine candidates owing to
447 their improved efficacy in comparison to subunit antigens [49, 50]. In the present study,
448 vaccination with the sVLPs resulted in enhanced humoral and cellular immune responses,
449 improving protection against an avian model of coronavirus infection as compared to free protein
450 antigens and a commercial WIV vaccine. Strong immunity against the viral challenge following
451 sVLP vaccination was evidenced by multiple criteria, including improved physical symptoms,
452 reduced organ lesions, and decreased overall viral load. The enhanced immunopotentiality by
453 the sVLPs is attributable at least in part to increased lymphatic delivery and multivalent antigen
454 display. Given the robustness and versatility of the approach, it can be envisioned the technique
455 can be broadly applied for different vaccine development.

456

457 **5. ACKNOWLEDGMENTS**

458 The study was supported by the Ministry of Science and Technology (103-2321-B-002-066, 104-
459 2321-B-002-023, 105-2321-B-001-055) and National Taiwan University (104R7320).

460

461 **6. REFERENCES**

- 462 [1] Moon JJ, Suh H, Li AV, Ockenhouse CF, Yadava A, Irvine DJ. Enhancing humoral
463 responses to a malaria antigen with nanoparticle vaccines that expand T-fh cells and
464 promote germinal center induction. *P Natl Acad Sci USA*. 2012;109:1080-1085.
465 [2] Bachmann MF, Jennings GT. Vaccine delivery: a matter of size, geometry, kinetics
466 and molecular patterns. *Nature Reviews Immunology*. 2010;10:787-796.
467 [3] Amanna IJ, Raue HP, Slifka MK. Development of a new hydrogen peroxide-based
468 vaccine platform. *Nature medicine*. 2012;18:974-979.

- 469 [4] Noad R, Roy P. Virus-like particles as immunogens. *Trends Microbiol.* 2003;11:438-
470 444.
- 471 [5] Kanekiyo M, Wei CJ, Yassine HM, McTamney PM, Boyington JC, Whittle JRR, et al.
472 Self-assembling influenza nanoparticle vaccines elicit broadly neutralizing H1N1
473 antibodies. *Nature.* 2013;499:102-106.
- 474 [6] Moon JJ, Suh H, Bershteyn A, Stephan MT, Liu HP, Huang B, et al. Interbilayer-
475 crosslinked multilamellar vesicles as synthetic vaccines for potent humoral and cellular
476 immune responses. *Nat Mater.* 2011;10:243-251.
- 477 [7] Hanson MC, Crespo MP, Abraham W, Moynihan KD, Szeto GL, Chen SH, et al.
478 Nanoparticulate STING agonists are potent lymph node-targeted vaccine adjuvants.
479 *The Journal of clinical investigation.* 2015;125:2532-2546.
- 480 [8] Nuhn L, Vanparijs N, De Beuckelaer A, Lybaert L, Verstraete G, Deswarte K, et al.
481 pH-degradable imidazoquinoline-ligated nanogels for lymph node-focused immune
482 activation. *Proc Natl Acad Sci U S A.* 2016;113:8098-8103.
- 483 [9] Fang RH, Hu CM, Luk BT, Gao W, Copp JA, Tai Y, et al. Cancer cell membrane-
484 coated nanoparticles for anticancer vaccination and drug delivery. *Nano Lett.*
485 2014;14:2181-2188.
- 486 [10] Tenzer S, Docter D, Kuharev J, Musyanovych A, Fetz V, Hecht R, et al. Rapid
487 formation of plasma protein corona critically affects nanoparticle pathophysiology.
488 *Nature nanotechnology.* 2013;8:772-781.
- 489 [11] Albanese A, Tang PS, Chan WC. The effect of nanoparticle size, shape, and
490 surface chemistry on biological systems. *Annual review of biomedical engineering.*
491 2012;14:1-16.
- 492 [12] Schottler S, Becker G, Winzen S, Steinbach T, Mohr K, Landfester K, et al. Protein
493 adsorption is required for stealth effect of poly(ethylene glycol)- and poly(phosphoester)-
494 coated nanocarriers. *Nature nanotechnology.* 2016;11:372-377.
- 495 [13] Li H, Fierens K, Zhang Z, Vanparijs N, Schuijs MJ, Van Steendam K, et al.
496 Spontaneous Protein Adsorption on Graphene Oxide Nanosheets Allowing Efficient
497 Intracellular Vaccine Protein Delivery. *ACS Appl Mater Interfaces.* 2016;8:1147-1155.
- 498 [14] Gao W, Fang RH, Thamphiwatana S, Luk BT, Li J, Angsantikul P, et al. Modulating
499 antibacterial immunity via bacterial membrane-coated nanoparticles. *Nano Lett.*
500 2015;15:1403-1409.
- 501 [15] Niikura K, Matsunaga T, Suzuki T, Kobayashi S, Yamaguchi H, Orba Y, et al. Gold
502 Nanoparticles as a Vaccine Platform: Influence of Size and Shape on Immunological
503 Responses in Vitro and in Vivo. *ACS nano.* 2013;7:3926-3938.
- 504 [16] Ghosh P, Han G, De M, Kim CK, Rotello VM. Gold nanoparticles in delivery
505 applications. *Advanced drug delivery reviews.* 2008;60:1307-1315.
- 506 [17] Cavanagh D. Coronavirus IBV: structural characterization of the spike protein. *The*
507 *Journal of general virology.* 1983;64 (Pt 12):2577-2583.
- 508 [18] Hilgenfeld R, Peiris M. From SARS to MERS: 10 years of research on highly
509 pathogenic human coronaviruses. *Antiviral research.* 2013;100:286-295.
- 510 [19] de Haan CA, Masters PS, Shen X, Weiss S, Rottier PJ. The group-specific murine
511 coronavirus genes are not essential, but their deletion, by reverse genetics, is
512 attenuating in the natural host. *Virology.* 2002;296:177-189.

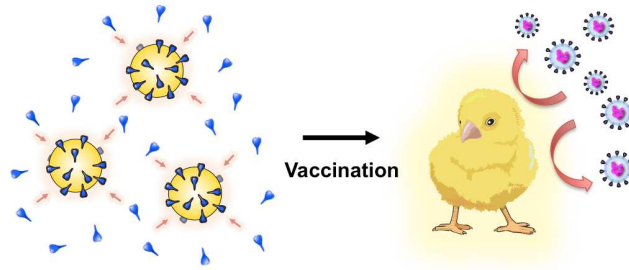
- 513 [20] Haijema BJ, Volders H, Rottier PJ. Live, attenuated coronavirus vaccines through
514 the directed deletion of group-specific genes provide protection against feline infectious
515 peritonitis. *J Virol.* 2004;78:3863-3871.
- 516 [21] Du L, Kou Z, Ma C, Tao X, Wang L, Zhao G, et al. A truncated receptor-binding
517 domain of MERS-CoV spike protein potently inhibits MERS-CoV infection and induces
518 strong neutralizing antibody responses: implication for developing therapeutics and
519 vaccines. *PloS one.* 2013;8:e81587.
- 520 [22] Coleman CM, Liu YV, Mu H, Taylor JK, Massare M, Flyer DC, et al. Purified
521 coronavirus spike protein nanoparticles induce coronavirus neutralizing antibodies in
522 mice. *Vaccine.* 2014;32:3169-3174.
- 523 [23] Chen HW, Wang CH, Cheng IC. A type-specific blocking ELISA for the detection of
524 infectious bronchitis virus antibody. *J Virol Methods.* 2011;173:7-12.
- 525 [24] Reed LJ, Muench H. A simple method of estimating fifty per cent endpoints.
526 *American Journal of Epidemiology.* 1938;27:493-497.
- 527 [25] Villegas P. Titration of biological suspensions. In: Swayne DE, Glisson JR,
528 Jackwood MW, Pearson JE, Reed WM, editors. *A Laboratory Manual for the Isolation
529 and Identification of Avian Pathogens.* Pennsylvania: The American Association of
530 Avian Pathologists; 1998. p. 248-254.
- 531 [26] Chen HW, Huang YP, Wang CH. Identification of Taiwan and China-like
532 recombinant avian infectious bronchitis viruses in Taiwan. *Virus Res.* 2009;140:121-
533 129.
- 534 [27] Docter D, Distler U, Storck W, Kuharev J, Wunsch D, Hahlbrock A, et al.
535 Quantitative profiling of the protein coronas that form around nanoparticles. *Nat Protoc.*
536 2014;9:2030-2044.
- 537 [28] Liu H, Zhang M, Han H, Yuan J, Li Z. Comparison of the expression of cytokine
538 genes in the bursal tissues of the chickens following challenge with infectious bursal
539 disease viruses of varying virulence. *Virol J.* 2010;7:364.
- 540 [29] Livak KJ, Schmittgen TD. Analysis of relative gene expression data using real-time
541 quantitative PCR and the 2(-Delta Delta C(T)) Method. *Methods.* 2001;25:402-408.
- 542 [30] Avellaneda GE, Villegas P, Jackwood MW, King DJ. In vivo evaluation of the
543 pathogenicity of field isolates of infectious bronchitis virus. *Avian Dis.* 1994;38:589-597.
- 544 [31] Huang YP, Lee HC, Cheng MC, Wang CH. S1 and N gene analysis of avian
545 infectious bronchitis viruses in Taiwan. *Avian Dis.* 2004;48:581-589.
- 546 [32] Jiang H, Yang H, Kapczynski DR. Chicken interferon alpha pretreatment reduces
547 virus replication of pandemic H1N1 and H5N9 avian influenza viruses in lung cell
548 cultures from different avian species. *Virol J.* 2011;8:447-458.
- 549 [33] Moerz ST, Kraegeloh A, Chanana M, Kraus T. Formation Mechanism for Stable
550 Hybrid Clusters of Proteins and Nanoparticles. *ACS nano.* 2015;9:6696-6705.
- 551 [34] Filipe V, Hawe A, Jiskoot W. Critical evaluation of Nanoparticle Tracking Analysis
552 (NTA) by NanoSight for the measurement of nanoparticles and protein aggregates.
553 *Pharmaceutical research.* 2010;27:796-810.
- 554 [35] Monopoli MP, Aberg C, Salvati A, Dawson KA. Biomolecular coronas provide the
555 biological identity of nanosized materials. *Nature nanotechnology.* 2012;7:779-786.
- 556 [36] Milani S, Bombelli FB, Pitek AS, Dawson KA, Radler J. Reversible versus
557 irreversible binding of transferrin to polystyrene nanoparticles: soft and hard corona.
558 *ACS nano.* 2012;6:2532-2541.

- 559 [37] Lundqvist M, Stigler J, Cedervall T, Berggard T, Flanagan MB, Lynch I, et al. The
560 evolution of the protein corona around nanoparticles: a test study. *ACS nano*.
561 2011;5:7503-7509.
- 562 [38] Reddy ST, van der Vlies AJ, Simeoni E, Angeli V, Randolph GJ, O'Neil CP, et al.
563 Exploiting lymphatic transport and complement activation in nanoparticle vaccines.
564 *Nature biotechnology*. 2007;25:1159-1164.
- 565 [39] Reddy ST, Berk DA, Jain RK, Swartz MA. A sensitive in vivo model for quantifying
566 interstitial convective transport of injected macromolecules and nanoparticles. *Journal of*
567 *applied physiology*. 2006;101:1162-1169.
- 568 [40] Heesters BA, Myers RC, Carroll MC. Follicular dendritic cells: dynamic antigen
569 libraries. *Nature reviews Immunology*. 2014;14:495-504.
- 570 [41] Belyakov IM, Ahlers JD. What Role Does the Route of Immunization Play in the
571 Generation of Protective Immunity against Mucosal Pathogens? *Journal of immunology*.
572 2009;183:6883-6892.
- 573 [42] Amanna IJ, Slifka MK. Contributions of humoral and cellular immunity to vaccine-
574 induced protection in humans. *Virology*. 2011;411:206-215.
- 575 [43] Cavanagh D. Coronavirus avian infectious bronchitis virus. *Vet Res*. 2007;38:281-
576 297.
- 577 [44] Du L, He Y, Zhou Y, Liu S, Zheng BJ, Jiang S. The spike protein of SARS-CoV--a
578 target for vaccine and therapeutic development. *Nat Rev Microbiol*. 2009;7:226-236.
- 579 [45] Lesniak A, Fenaroli F, Monopoli MP, Aberg C, Dawson KA, Salvati A. Effects of the
580 presence or absence of a protein corona on silica nanoparticle uptake and impact on
581 cells. *ACS nano*. 2012;6:5845-5857.
- 582 [46] Walkey CD, Olsen JB, Song F, Liu R, Guo H, Olsen DW, et al. Protein corona
583 fingerprinting predicts the cellular interaction of gold and silver nanoparticles. *ACS*
584 *nano*. 2014;8:2439-2455.
- 585 [47] Walkey CD, Chan WC. Understanding and controlling the interaction of
586 nanomaterials with proteins in a physiological environment. *Chem Soc Rev*.
587 2012;41:2780-2799.
- 588 [48] Nel AE, Madler L, Velegol D, Xia T, Hoek EMV, Somasundaran P, et al.
589 Understanding biophysicochemical interactions at the nano-bio interface. *Nat Mater*.
590 2009;8:543-557.
- 591 [49] Wang C, Zheng X, Gai W, Zhao Y, Wang H, Wang H, et al. MERS-CoV virus-like
592 particles produced in insect cells induce specific humoral and cellular immunity in
593 rhesus macaques. *Oncotarget*. 2016.
- 594 [50] Liu G, Lv L, Yin L, Li X, Luo D, Liu K, et al. Assembly and immunogenicity of
595 coronavirus-like particles carrying infectious bronchitis virus M and S proteins. *Vaccine*.
596 2013;31:5524-5530.

597

598

599

600 **TABLE OF CONTENTS (TOC) GRAPHIC**

601

602

603

604

ACCEPTED MANUSCRIPT